

Bone substitute: Transforming β -tricalcium phosphate porous scaffolds into monetite

Laëtitia G. Galea^{a,b}, Marc Bohner^{a,*}, Jacques Lemaître^b, Thomas Kohler^c, Ralph Müller^c

^aDr Robert Mathys Foundation, Bischmattstrasse 12, CH-2544 Bettlach, Switzerland

^bPowder Technology Laboratory, Swiss Federal Institute of Technology of Lausanne (EPFL), EPFL-STI-IMX-LTP, MXD 337 (Bâtiment MXD), Station 12, CH-1015 Lausanne, Switzerland

^cInstitute for Biomechanics, ETH Zurich, Wolfgang-Pauli-Strasse 10, CH-8093 Zurich, Switzerland

ARTICLE INFO

Article history:

Received 11 March 2008

Accepted 23 April 2008

Available online 20 May 2008

Keywords:

Calcium phosphate

Calcium phosphate cement

Scaffold

Crystallization

Compression

Ceramic structure

ABSTRACT

The goal of the present study was to assess the possibility to change the composition of a calcium phosphate scaffold from a high-temperature phase to a phase only stable at or close to room temperature without macrostructural changes. For that purpose, macroporous β -TCP scaffolds were converted into α -TCP by high-temperature thermal treatment and then dipped into a phosphoric acid solution to obtain a more acidic calcium phosphate phase called monetite or dicalcium phosphate (DCP; CaHPO_4). Two different solid-to-liquid ratios (SLR: 0.067 and 0.200 g/mL) and three different temperatures (T : 37, 60 and 80 °C) were used. The reaction was followed by measuring the change of sample size and weight, by determining the compositional changes by X-ray diffraction (Rietveld analysis), and by looking at the micro- and macrostructural changes by scanning electron microscopy and micro-computed tomography. The results revealed that the transformation proceeded faster at a higher temperature and a higher SLR value but was achieved within a few days in all cases. Morphologically, the porosity decreased by 10%, the pore size distribution became wider and the mean macro pore size was reduced from 0.28 to 0.19 mm. The fastest conversion and the highest compressive strength (9 MPa) were measured using an incubation temperature of 80 °C and an SLR value of 0.2 g/mL.

© 2008 Elsevier Ltd. All rights reserved.

1. Introduction

The most common strategy used to heal bone defects resulting from trauma or diseases is to fill the defect with autologous bone, typically from the iliac crest. Unfortunately, this technique has several drawbacks such as the need for a second surgery that prolongs the surgical operation and an increased risk of side-effects such as infections or pain [1,2]. One alternative to bone grafts is the use of synthetic calcium phosphate substitutes [3]. These materials have generally a composition very close to that of the mineral part of bone and as a result present excellent biological properties such as biocompatibility, osteoconduction (ability to lead bone formation) and osteotransduction (replacement of the material by new bone).

Most calcium phosphate bone substitutes sold commercially are obtained by thermal treatments at high temperature (>1000 °C) via a so-called sintering reaction. These materials include β -tricalcium phosphate (β -TCP; $\text{Ca}_3(\text{PO}_4)_2$), sintered hydroxyapatite (HA; $\text{Ca}_5(\text{PO}_4)_3\text{OH}$) or their composites called biphasic calcium phosphates [4]. In 1983, Brown and Chow [5] demonstrated that specific mixtures of calcium phosphate powders could react with water and

harden in a very similar way to the reaction of Plaster of Paris to form gypsum. The discovery of calcium phosphate cements (CPCs) led to the publication of thousands of papers and to more than a dozen commercial formulations [6].

Despite the fact that CPC has very interesting handling properties such as the possibility to be injected, to fill any defect shape, and to provide a certain mechanical stability, most bone substitutes are still sold under the form of small granules (typically 0.1–5 mm in diameter) [7]. This fact results from the lower cost and better biological properties of granules compared to CPCs: whereas CPCs are seen essentially as compact materials by cells [8], the space between granules can be easily invaded and colonized by blood vessels and bone cells [9]. These cells are able to rapidly resorb the granules and replace them with mature bone.

In the last decade, several researchers recognized the interest of using CPCs to synthesize granules and porous blocks [10,11]. This decision was governed by the combination of two very important features of CPC: first, scaffolds produced from CPC do not necessitate any further sintering to be used as bone substitute as the cement reaction already provides an important mechanical stability [12]; second, their composition and structure are very close (if not identical) to the calcium phosphate compounds found in the body such as dicalcium phosphate dihydrate (DCPD; $\text{CaHPO}_4 \cdot 2\text{H}_2\text{O}$), octocalcium phosphate (OCP; $\text{Ca}_8\text{H}_2(\text{PO}_4)_6 \cdot 5\text{H}_2\text{O}$), and carbonated

* Corresponding author. Tel.: +41 326441413; fax: +41 326441176.

E-mail address: marc.bohner@rms-foundation.ch (M. Bohner).

apatite [13]. These similarities, in particular the large specific surface area of these compounds, is believed to bring an improvement of the already excellent biological responses of calcium phosphate compounds [14]. In vivo results of these compounds are indeed very promising [15–17], but the potential benefit of a higher specific surface area still remains to be demonstrated.

Unfortunately, there are two drawbacks in the use of CPC for scaffold synthesis, namely the risk of microbial contamination during the (wet) synthesis process that can potentially lead to biocompatibility problems during implantation (pyrogenicity) and their relatively low mechanical properties due to large porosities. Here a new synthesis method is proposed that can potentially solve both problems.

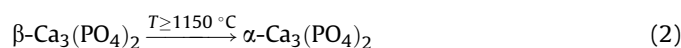
Until now, macroporous scaffolds (macropore = pore with a diameter larger than 0.05 mm) produced with CPC have been produced by combining the shaping process with the CPC reaction. More specifically, authors mixed the CPC powders or paste with a secondary phase such as solid particles [10,18], an insoluble liquid phase [11] or a gas or gas-forming phase [19], let the material harden, and then removed the secondary phase (if necessary) to obtain a macroporous scaffold. Here, it is proposed to give the final shape of the scaffold before the CPC reaction and then adjust the chemistry. For that purpose, macroporous scaffolds were produced beforehand, transformed into a reactive compound by high-temperature thermal treatment and then converted into the desired composition. To assess the feasibility of this approach, scaffolds made of β -TCP were used and converted into a more acidic calcium phosphate phase called monetite or dicalcium phosphate (DCP; CaHPO_4).

DCP is an interesting calcium phosphate compound. Its solubility product is very close to the solubility product of serum, and as a result, this compound has been seen to rapidly resorb and transform into bone [17,20–22].

Two chemical routes can be used to convert β -TCP into DCP. In the first route, β -TCP is reacted with phosphoric acid according to reaction (1):



In the second route, β -TCP is first converted into α -tricalcium phosphate (α -TCP; $\alpha\text{-Ca}_3(\text{PO}_4)_2$) using a thermal treatment above 1150 °C (reaction (2)) [23]. Then, the more reactive α -TCP is converted to DCP according to reaction (3):



In this study, only the second route proved to work well. In the first route, the edges of the β -TCP samples were dissolved under the action of phosphoric acid and the initial sample shape was lost during the reaction. Therefore, in the following the results obtained applying the second chemical route will be described, i.e. the thermal conversion of β -TCP into α -TCP followed by the chemical conversion of α -TCP into DCP.

2. Materials and methods

For practical reasons, the β -TCP cylinders were produced according to a method commonly used by the authors and previously reported [11,24]. The only difference with the reported method was the choice of a different sintering temperature (1200 °C instead of 1250 °C) and geometry ($\theta = L = 7$ mm, instead of $\theta = 8$ mm, and $L = 13$ mm). The cylinders had a total porosity of $74 \pm 1\%$ with a macroporosity (macropores larger than 0.05 mm) close to 54% (assessed from the oil volume fraction in the initial paste; for more details, see Ref. [24]).

Five different batches of eight large cylinders (20–30 mL each) were produced at once and used to produce a few hundred cylinders. Even though the sample

homogeneity was very high (either within a batch or between batches), the cylinders were randomized.

The conversion of β -TCP into α -TCP was performed at 1500 °C for 4 h in a muffle furnace (heating rate: 5 °C/min; Nabertherm, LHT 02/16; Germany). About 150 blocks stood vertically on a calcium-stabilized ZrO_2 plate (S-3406, Zircoa, USA). At the end of the selected sintering time, the plate on which the blocks were standing was taken out of the furnace to achieve very rapid cooling.

The conversion of α -TCP cylinders into DCP cylinders was performed in 2 mL Eppendorf tubes (for a solid-to-liquid ratio (SLR) of 0.200 g/mL) or 5 mL plastic tubes (for SLR = 0.067 g/mL). In each tube, a given volume of phosphoric acid solution was added to one single α -TCP cylinder (~ 0.2 g) and incubated for a pre-defined duration at a pre-defined temperature. The experimental factors that were varied were: (A) temperature (T : 37, 60 and 80 °C); (B) solid-to-liquid ratio (SLR: 0.067 and 0.200 g/mL – the phosphoric acid solution had a concentration of 0.233 and 0.700 M, respectively); and (C) incubation time (t : 200 s, 30 min, 4.5, 48 h). At the end of the incubation period, the samples were removed from the Eppendorf tubes, placed on an absorbing paper, soaked in ethanol, and placed again on absorbing paper. The latter rinsing procedure was repeated twice with water. Finally, the samples were dried at 60 °C until constant weight was reached. Five samples of each composition were produced leading to a total of 3 temperatures \times 2 SLR \times 4 incubation times \times 5 repeats = 120 samples.

Block characterizations included: (i) weighing and size measurements to determine the apparent volume, apparent density and porosity; (ii) micro-computed tomography (μCT) to determine the macropore size distribution; (iii) mechanical testing to determine the compressive strength; (iv) nitrogen adsorption to determine the specific surface area (SSA) using the BET model; (v) scanning electron microscopy (SEM) to assess the nano-, micro-, and macrostructure; and (vi) X-ray diffraction (XRD) to assess the crystalline composition. The details of some of the characterization methods are given hereafter. Importantly the terminology used in the present work to define pores is the following: nanopore = pore in the nanosize range, i.e. smaller than 1 μm in diameter; micropore = pore between 1 and 50 μm in diameter; and macropore = pore larger than 50 μm in diameter. The latter size can be considered to be close to the minimum diameter that a pore should have to be accessed by cells.

The characterizations were performed in a pre-defined order. Before processing, each block was weighed and its size was measured to determine the apparent density. Four samples were analyzed by micro-computed tomography (μCT 40, Scanco Medical AG, Brüttisellen, Switzerland) before transformation to α -TCP, after transformation to α -TCP and after transformation to monetite. A microfocus X-ray tube with a focal spot of 7 μm was used as a source. Measurements were stored in a three-dimensional image arrays with an isotropic voxel size of 10 μm . Besides assessing visually the block images, morphometric parameters were determined from the μCT datasets using direct 3D morphometry [25,26]. Each of the four samples analyzed by μCT was submitted to different incubation conditions: the incubation temperature was either 60 or 80 °C and the SLR value was either a 0.067- or 0.200-g/mL. The SSA was measured by nitrogen adsorption using the BET model (Gemini 2360, Micromeritics, USA). Four samples were tested per composition and time. As the block diameter was smaller than the testing tube diameter (>7 mm), the blocks could be directly inserted into the test tubes. All five samples with the same treatment were then mechanically tested at a compressive load rate of 0.5 mm/min (Zwick 1474, Zwick, Ulm, Germany). Afterwards, one sample per group was characterized by XRD. For that purpose, the block was ground to obtain a powder. The powder was homogenized and packed in a cavity in an aluminum sample holder. XRD data were collected in reflective geometry on a Philips PW1800 diffractometer (Philips, Eindhoven, The Netherlands) equipped with a graphite monochromator in the secondary beam. $\text{CuK}\alpha$ radiation and a step size of 0.02° were used to measure from 4.01 to $59.99^\circ 2\theta$. Rietveld refinements for quantitative phase analysis were done with the computer program FullProf.2k (Version 3.40) [27] using a previously determined instrument resolution function. Starting models for the quantified phases were taken from Ref. [28] for β -TCP (whitlockite model, but with fully Ca-occupied sites), Ref. [29] for α -TCP, Ref. [30] for monetite, and Ref. [31] for brushite. For SEM, one sample per composition and reaction time was coated with gold and observed with a Cambridge S360 microscope (Leica, Germany).

3. Results

The SEM analysis of the samples clearly demonstrated the presence of micro- and macropores in the samples, and revealed that the micro- and macrostructure of the samples were not markedly modified during the various reactions (Fig. 1). However, small changes were noticed. For example, the macropores appeared smaller and the microstruts appeared thicker after the thermal treatment used to convert β -TCP into α -TCP (compare Fig. 1a,e and b, f). A more important change was seen during the conversion of α -TCP to DCP: after only 200 s of reaction, the micropores were not only filled with fine crystals, but also the macropore walls were covered with crystals varying in size and shape (Fig. 1c,g,k; Fig. 2).

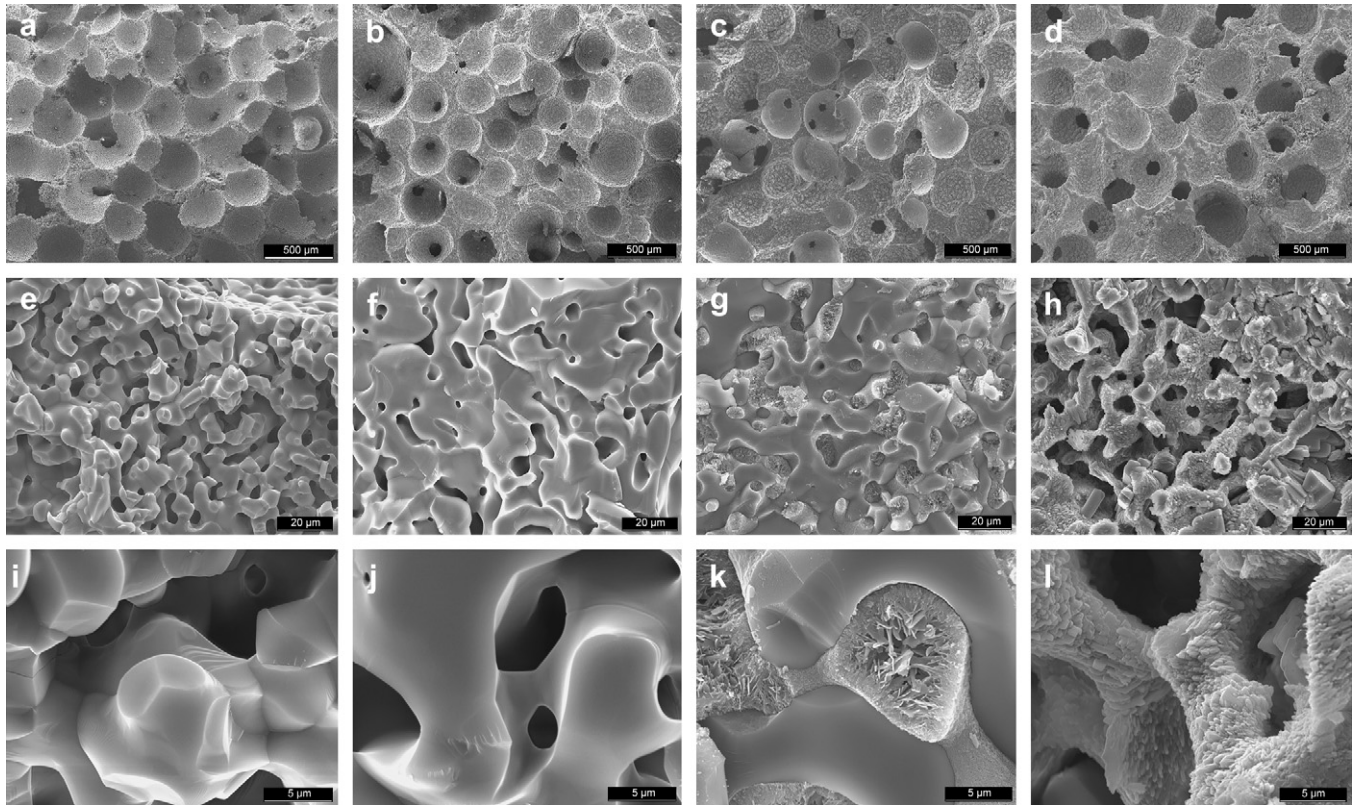


Fig. 1. Microstructure of the blocks as seen by SEM before transformation to α -TCP (left column; Fig. 1a,e,i), after transformation to α -TCP (middle-left column; Fig. 1b,f,j), after reacting the α -TCP blocks for 200 s in phosphoric acid solution (middle-right column; Fig. 1c,g,k), and after reacting the α -TCP blocks for 2 days in phosphoric acid solution (right column; Fig. 1d,h,l). SLR = 0.20 g/mL. Conversion temperature: 80 °C. Error bar: on top: 500 μ m (Fig. 1a–d); in the middle: 20 μ m (Fig. 1e–h); and at the bottom: 5 μ m (Fig. 1i–l).

After 2 days of reaction, the microstructure initially defining the microporosity had disappeared in some places while the initially empty micropores were completely filled with a fine crystalline structure (Fig. 1d,h,l). In other words, the conversion of α -TCP to DCP replaced the microporous structure by its negative (also microporous) structure (Fig. 1h).

Few macroscopic changes were seen by μ CT during the two phase conversions (Fig. 3). The main change was a partial filling of the macropores during the transformation of α -TCP to DCP. A closer look at one specific location of a block (Fig. 4) shows that the macropore size was reduced during the first phase transformation and partly filled with new material during the second phase transformation. These observations were confirmed by the analysis

of the pore size distribution (Fig. 5, Table 1). Importantly, μ CT images did not reveal the presence of micropores (Fig. 3).

The apparent volume of the samples was calculated based on the diameter and height of the (cylindrical) samples assuming that the shape remained constant during the conversion of α -TCP into DCP. The latter assumption was not always 100% true since the shape tended to change at the contact surface between plastic tube and block. During the transformation of β -TCP in α -TCP scaffolds, the apparent volume decreased from 0.266 ± 0.003 to 0.234 ± 0.010 mL. The latter value was hardly changed during the conversion of α -TCP into DCP. In fact, only one factor had a significant effect at $p < 0.01$, namely the interaction between the SLR value and the time (data not shown here). The effect was linear and all estimated values were in

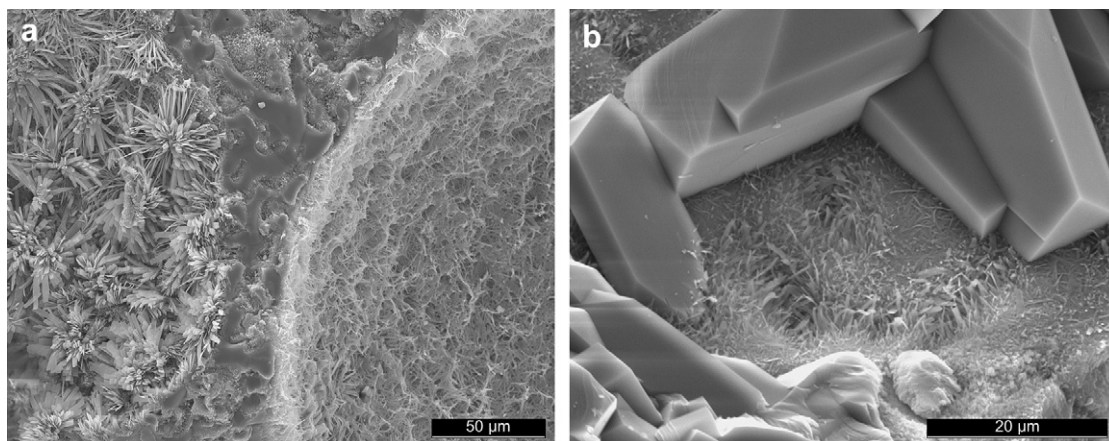


Fig. 2. DCP crystals seen at macropore surfaces. These photos show that large changes of crystal size and shape are found within the same sample: (a) a ruptured surface shows the size and shape of DCP crystals in two different macropores (left and right side of the photo); (b) size and shape of DCP crystals within a macropore.

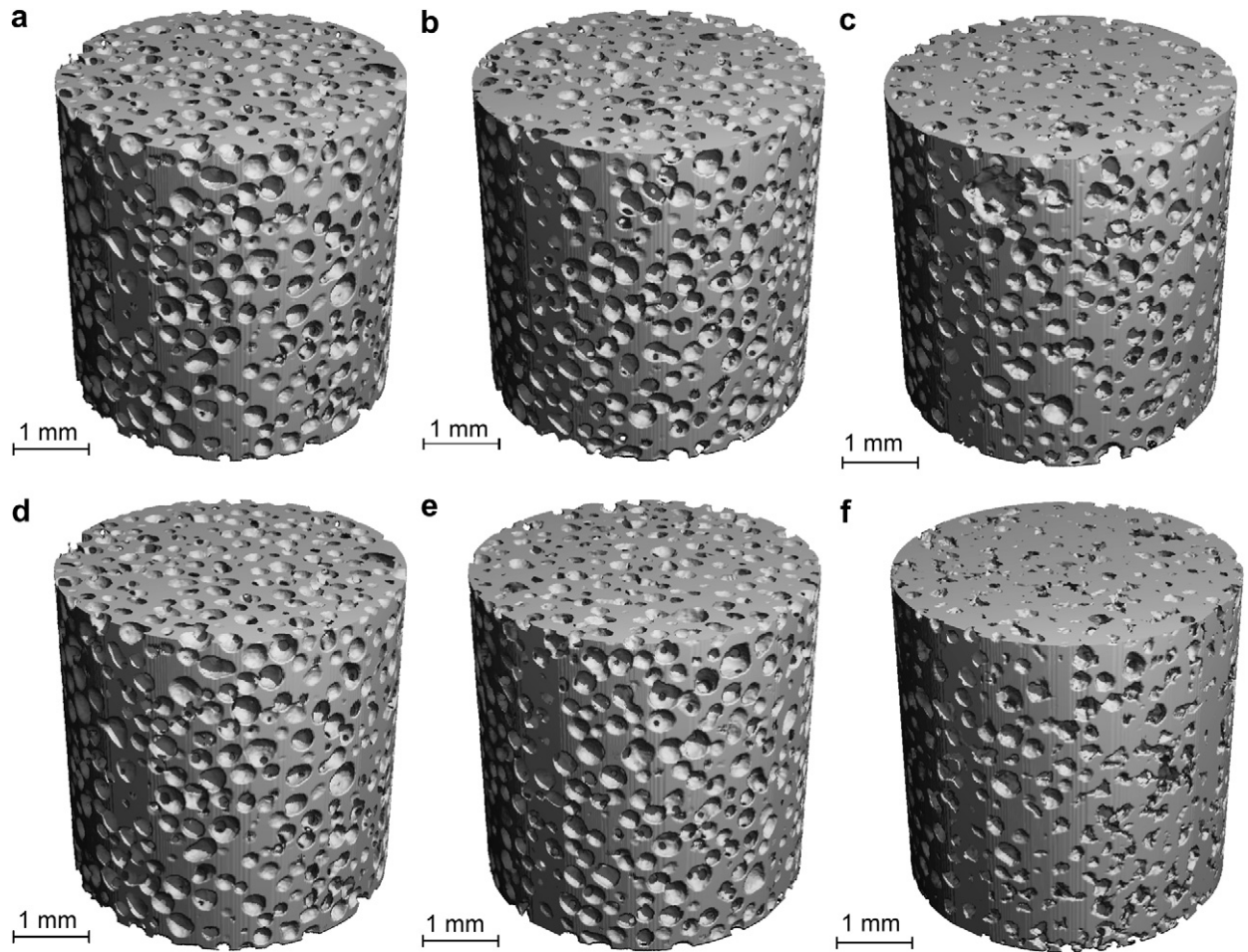


Fig. 3. Morphological changes of four blocks during phase transformation as seen by μ CT. Left column: before conversion to α -TCP; middle column: after conversion to α -TCP; and right column: after 2-day conversion to DCP. Top row: SLR = 0.200 g/mL; 60 °C; bottom row: SLR = 0.067 g/mL; 80 °C.

the range of 0.220 ± 0.021 and 0.234 ± 0.021 mL. More specifically, the apparent volume decreased from 0.234 ± 0.021 to 0.220 ± 0.021 mL at an SLR value of 0.067 g/mL when the reaction time increased from 200 s to 2 days. The evolution at an SLR value of 0.200 g/mL was exactly the opposite (from 0.220 ± 0.021 to 0.234 ± 0.021 mL).

The apparent density of the samples increased significantly with time ($p < 0.01$) during the conversion of β -TCP into α -TCP and during that of α -TCP into DCP (Fig. 6a). Interestingly, the change of apparent density during the conversion of α -TCP into DCP was linear with $\log(t)$ and was not significantly affected by the SLR value or temperature. The values ranged from 0.74 ± 0.04 g/cc (± 1 SD) for

β -TCP to 0.83 ± 0.02 g/cc at time zero (α -TCP) and 1.05 g/cc after 2 days of reaction in phosphoric acid. A significant ($p < 0.01$) but opposite trend was observed for the porosity (Fig. 6b). The values decreased from $74 \pm 1\%$ (± 1 SD) for β -TCP to $71 \pm 1\%$ for α -TCP (time zero of the reaction) and $64 \pm 1\%$ after 2 days of reaction.

According to XRD, DCP was formed very rapidly (Figs. 7 and 8). First diffraction peaks were already observed after 200 s of reaction (Fig. 7) and the reaction was complete after 2 days at 60 and 80 °C for SLR = 0.2 g/mL (Fig. 8). Interestingly, the samples incubated at 37 °C contained some brushite, contrary to those incubated at the two highest temperatures. Another important point is the fact that more α -TCP remained in the samples incubated at the lowest SLR,

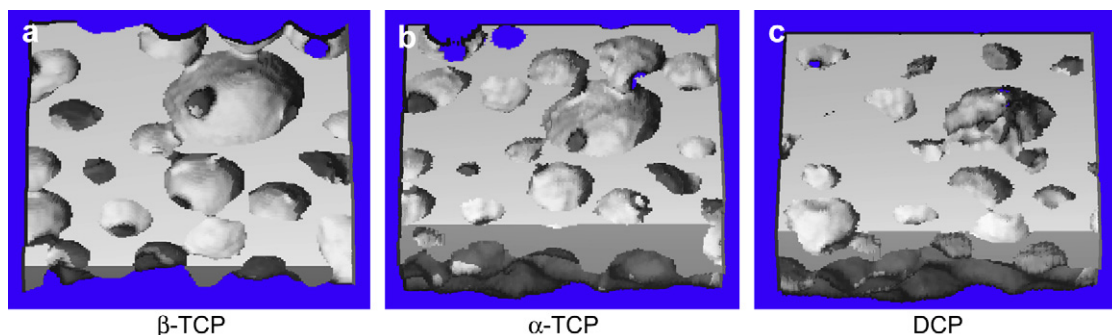


Fig. 4. Evolution of the porous structure in one particular location of one sample. SLR = 0.067 g/mL; $T = 60$ °C. (a) Before conversion to α -TCP; (b) after conversion to α -TCP; and (c) after 2-day conversion to DCP.

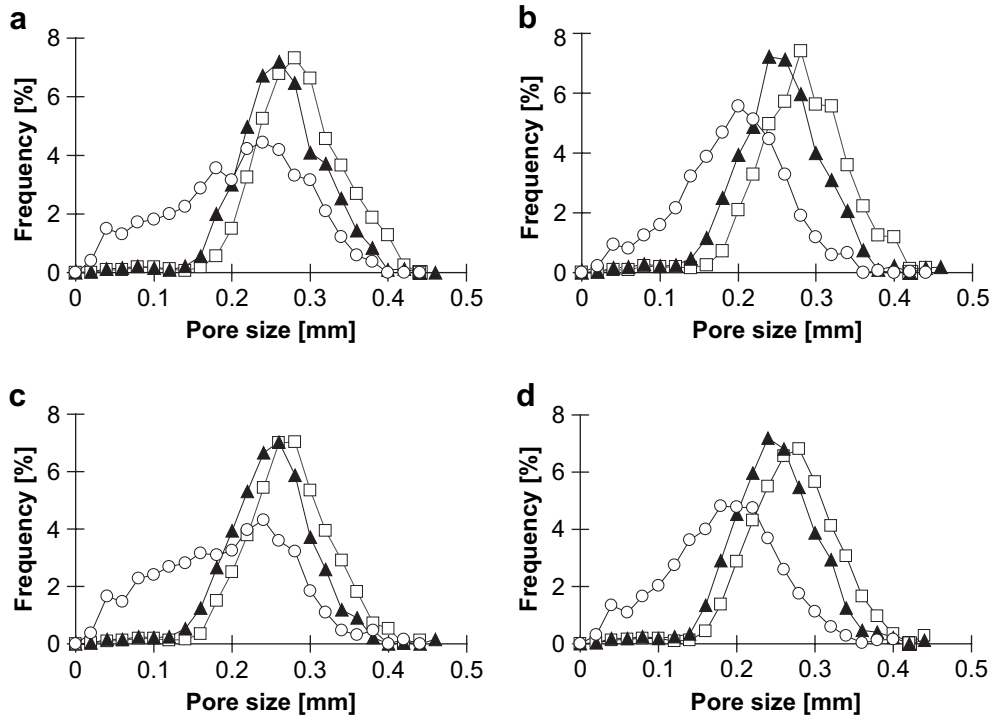


Fig. 5. Evolution of the pore size distribution and size distribution of the pore interconnections. (a) SLR = 0.067 g/mL; 60 °C; (b) SLR = 0.200 g/mL; 60 °C; (c) SLR = 0.067 g/mL; 80 °C; and (d) SLR = 0.200 g/mL; 80 °C. Symbols: (□) before conversion to α -TCP; (▲) after conversion to α -TCP; and (○) after 2-day conversion to DCP.

suggesting a slower reaction. However, only one sample per composition and time was analyzed by XRD, so that no statistically significant changes could be observed.

The samples SSA increased from 0.22 ± 0.02 to $4\text{--}5 \text{ m}^2/\text{g}$ within 200 s (Fig. 9). Beyond that point, the SSA of blocks was significantly influenced by many factors and interactions of factors. In particular, both the reaction time and the interaction between reaction time and SLR value had a quadratic effect.

The compressive strength of the blocks was positively influenced by the transformation of β -TCP into α -TCP (from 4 to 6 MPa) even though this effect was not significant at $p < 0.01$. The conversion of α -TCP into DCP affected the compressive in a more complex way (Fig. 10) as not only the main effects of SLR and temperature but also their interaction were significant ($p < 0.01$). At an SLR value of 0.067 g/mL, compressive strengths ranged between 4 and 5 MPa with only a minor increase at increasing temperatures. At an SLR value of 0.200 g/mL, the strength increased

linearly from below 4 MPa at 37 °C to 9 MPa at 80 °C. Interestingly, the reaction time did not significantly affect the results.

4. Discussion

The goal of the present study was to assess whether it is possible to convert β -TCP scaffolds into DCP scaffolds without major morphological changes. Generally, the results presented in this study support this statement, but require additional explanations.

Ideally, the sample geometry should not change during the conversion of β -TCP into DCP blocks to eliminate the need of machining the samples after conversion. Here, despite the fact that the apparent volume of α -TCP scaffolds was practically not modified during the transformation of α -TCP into DCP, size changes were seen when β -TCP scaffolds were converted into α -TCP scaffolds (from 0.266 ± 0.003 to 0.234 ± 0.010 mL). To prevent this, one possibility could be to use a higher sintering temperature for β -TCP scaffolds (e.g. 1500 °C instead of 1200 °C).

The analysis of the SEM pictures revealed that the morphology of the crystals formed at macropore surfaces varied extensively within samples and less from sample to sample (Figs. 1 and 2). Two explanations can be proposed. Firstly, since the phosphoric acid solution was not degassed before mixing and since mixing was not performed under vacuum, it is possible that some of the macropores contained air bubbles. Secondly, due to the microporous nature of the scaffolds and the limited presence of macropore interconnections, the solution composition was certainly different inside and outside the block. As a result, there was probably a composition gradient between the outer and the inner part. Indeed, the crystalline composition of one sample was determined and showed significant differences between its external surface and its core (40 and 20% DCP, respectively).

The various SEM and μ CT pictures (Figs. 1–4) show that the scaffold microstructure was more affected than its macrostructure. In fact, this is quite likely to happen if the whole scaffold surface reacts in a similar way. The formation of a small DCP layer at the

Table 1

Results of the μ CT analysis before conversion to α -TCP (Time 1), after conversion to α -TCP (Time 2), and after conversion to DCP (Time 3)

Treatment	Response	Time 1	Time 2	Time 3
60 °C, 0.067 g/mL	Porosity [%]	51	48	35
	Mean pore size [mm]	0.28 ± 0.06	0.26 ± 0.06	0.20 ± 0.08
60 °C, 0.200 g/mL	Porosity [%]	51	47	33
	Mean pore size [mm]	0.28 ± 0.07	0.25 ± 0.07	0.19 ± 0.08
80 °C, 0.067 g/mL	Porosity [%]	50	47	38
	Mean pore size [mm]	0.27 ± 0.08	0.25 ± 0.08	0.19 ± 0.10
80 °C, 0.200 g/mL	Porosity [%]	50	46	33
	Mean pore size [mm]	0.27 ± 0.06	0.24 ± 0.06	0.18 ± 0.07

Only one sample was analyzed per treatment. The errors indicated in the table correspond to ± 1 SD. The average porosity of the four samples was 51 ± 1 , 47 ± 1 , and $35 \pm 2\%$ at Time 1, 2 and 3, respectively. The average pore size of the four samples was 0.28 ± 0.01 , 0.25 ± 0.01 , and 0.19 ± 0.01 mm at Time 1, 2 and 3, respectively.

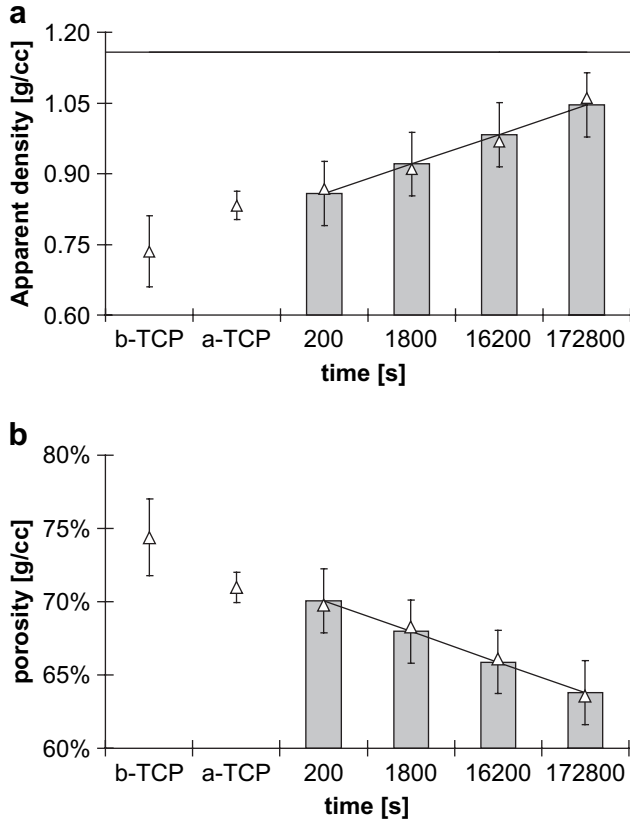


Fig. 6. Evolution of (a) the apparent density and (b) the porosity of the samples during the conversion reaction of α -TCP into DCP. Incubation times are expressed in seconds and correspond to 3 min 20 s (=200 s), 30 min (=1800 s), 4 h 30 min (=16,200 s), and 48 h (=172,800 s). The bars correspond to the values adjusted according to the statistical model, whereas the symbols (Δ) correspond to the average values. The error bars correspond to the 99% confidence interval of the adjusted values. Fit: (a) apparent density = $6.76 - 3.69 \times 10^{-2} \times \log(t)$; (b) porosity = $75.0 - 2.13 \times \log(t)$. The horizontal line on Fig. 6a corresponds to the apparent density that is expected applying Eq. (3) (assuming the absence of calcium and phosphate ions in the mixing solution).

solid–micropore interface would completely fill the micropore, whereas the same reaction at the solid–macropore interface would only slightly reduce the macropore size. Such a phenomenon coupled to an inhomogeneous reaction rate might explain why the pore size distribution not only decreased during the conversion of α -TCP into DCP, but also became wider (Fig. 5).

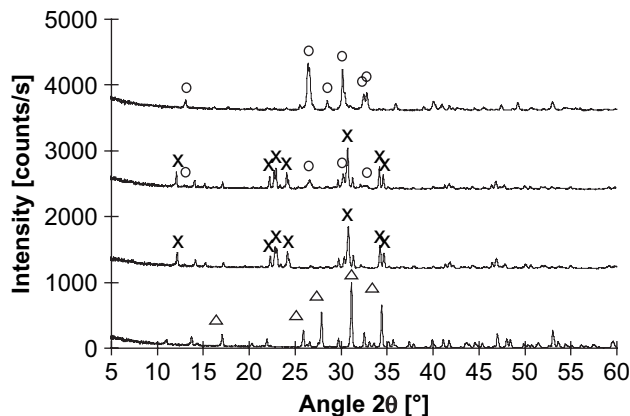


Fig. 7. XRD patterns. The main peaks corresponding to (Δ) β -TCP, (\times) α -TCP and (\circ) DCP are represented. Spectra from bottom to top: before conversion to α -TCP; after conversion to α -TCP; after 3 min 20 s of incubation (SLR = 0.200 g/mL; $T = 60^\circ\text{C}$) and after 2 days of incubation (SLR = 0.200 g/mL; $T = 60^\circ\text{C}$).

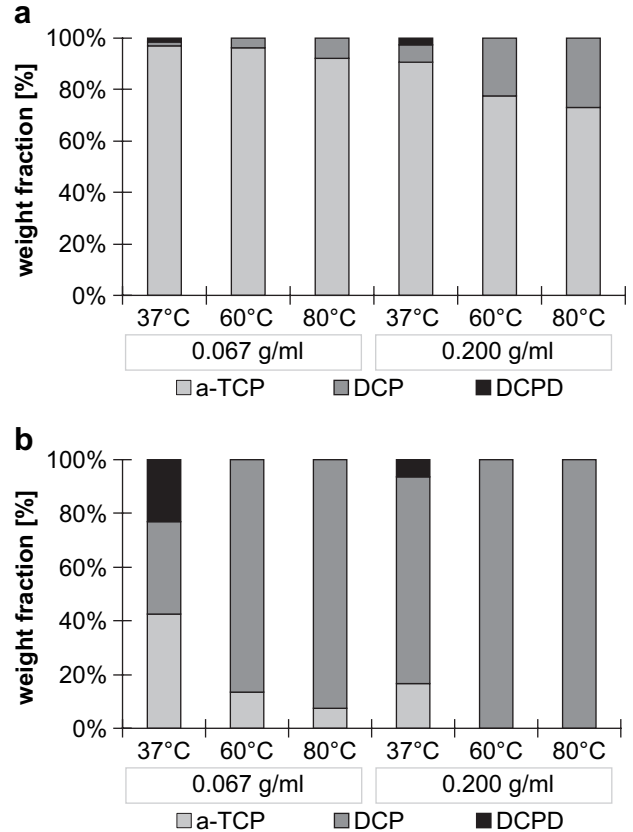


Fig. 8. Crystalline composition of the samples according to XRD Rietveld analysis. (a) After 200 s of reaction; (b) after 2 days of reaction. Only one sample was analyzed per condition.

No information is provided here regarding to the size of pore interconnections, even though interconnections play a major role in the biological response of bone substitutes [32–35]. The SEM photos shown in Fig. 2 suggest that the number and size of the interconnections were not markedly changed. This point should be looked at more carefully in the future.

The scaffold porosity measured using their weight and size was close to 70% whereas those measured by μCT was close to 40–50% (Table 1). The reason for this discrepancy is related to the relatively low resolution of μCT ($10 \times 10 \times 10 \mu\text{m}^3$) compared to the size of the micropores (close to $<10 \mu\text{m}$; Fig. 1). As a result, only macropores could be detected by μCT . The macroporosity of the β -TCP samples used in this study was close to 54%, i.e. close to the values measured here after phase conversion. The decrease of porosity during the first and the second transformation is probably related on one side to the decrease of mean macropore size, hence resulting in a more difficult detection of macropores (Fig. 5) and on the other side to a decrease of the overall porosity due to filling of macropores with DCP (Fig. 6b).

The apparent density of the samples did not reach a value of 1.16 g/cc predicted by reaction (3) assuming a constant apparent volume (Fig. 6a). In fact, reaction (3) assumes that the solution contains only water at the end of the reaction even though DCP is a fairly soluble compound in slightly acidic conditions [36]. As the final pH values of the incubating solutions were all in the range of 2.54–2.83, it is likely that non-neglectable amounts of calcium and phosphate ions present in the incubating solution were removed during the washing step performed at the end of incubation, hence resulting in lower-than-expected apparent density values.

The rate of the α -TCP–DCP conversion reaction was enhanced with an increase of temperature and SLR value. Apparently, the

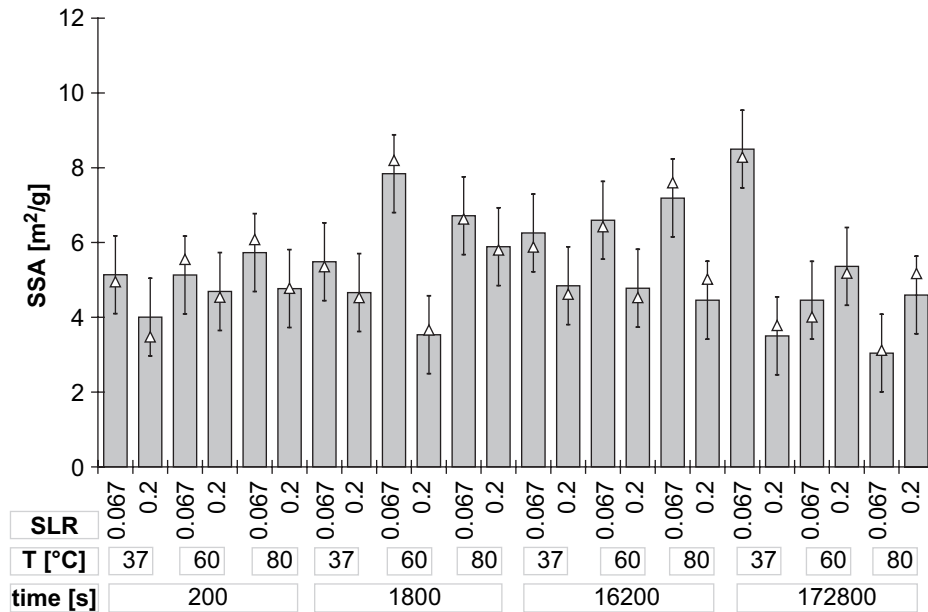


Fig. 9. Evolution of the block SSA during α -TCP conversion to DCP. Incubation times are expressed in seconds and correspond to 3 min 20 s (=200 s), 30 min (=1800 s), 4 h 30 min (=16,200 s), and 48 h (=172,800 s). The bars correspond to the values adjusted according to the statistical model, whereas the symbols (Δ) correspond to the average values. The error bars correspond to the 99% confidence interval of the adjusted values.

benefit of larger diffusion rates at higher temperature was higher than the drawback of having lower solubilities [36]. The effect of the SLR is probably due to the fact that the solubility of α -TCP was higher in the more acidic 0.700 M phosphoric acid solution used for an SLR value of 0.2 g/mL than in the less acidic 0.233 M phosphoric acid solution used for an SLR of 0.067 g/mL.

The presence of brushite in samples incubated at 37 °C was unexpected because DCP is less soluble than brushite at all pH values and temperatures [36]. However, brushite formation is kinetically favored compared to that of DCP, particularly at low temperatures [37–39]. Importantly, the crystalline composition of the samples was determined after drying even though it has been reported that brushite can convert to DCP, particularly in humid and slightly acidic conditions [40–43]. Therefore, it is possible that the brushite content was larger at the time of reaction, but decreased during drying.

As previously seen, the SSA results are very simple and very complex at the same time (Fig. 9). The simple part is the fact that

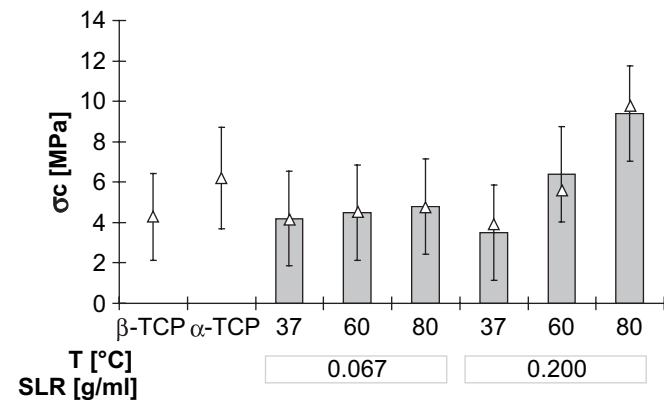


Fig. 10. Evolution of the compressive strength during the transformation of β -TCP to DCP. Incubation times are expressed in seconds and correspond to 3 min 20 s (=200 s), 30 min (=1800 s), 4 h 30 min (=16,200 s), and 48 h (=172,800 s). The bars correspond to the values adjusted according to the statistical model, whereas the symbols (Δ) correspond to the average values. The error bars correspond to the 99% confidence interval of the adjusted values.

the replacement of large rounded α -TCP surfaces by fine DCP crystals (Figs. 1 and 2) led to a rapid and roughly 20-fold SSA increase (from 0.22 to about 4–5 m²/g). The complex part is the fact that many factors and interactions of factors played a significant role (at $p < 0.01$) on the SSA values (Fig. 9). In particular, both the reaction time and the interaction between reaction time and SLR value had a quadratic effect. These results are likely to be related to the fact that the DCP content increases with time, which should lead to an increase of SSA, and that the DCP crystal size is expected to increase with time, which should decrease the SSA.

Scaffolds used in surgery should not only have the right composition and structure, but also present a mechanical strength high enough as to stand surgical handling. A compressive strength larger than 1–2 MPa is sufficient in most cases. Here, the conversion of β -TCP scaffolds into DCP had no negative effect on the compressive strength. In fact, the values were increased two-fold up to 9 MPa with an SLR value of 0.2 g/mL and an incubation temperature of 80 °C. It is clear that a simple compressive test is not sufficient to fully characterize the samples mechanically [44], but provides enough information since the scaffolds are not meant to be implanted in load bearing areas (considering the fragile nature of calcium phosphate bone substitute, it is a contra-indication).

One important goal of the present study was to provide a method that would allow producing scaffolds made of a calcium phosphate phase only stable at or close to room temperature (e.g. DCP) in pyrogene-free conditions. Here, conversion was performed using high-temperature pyrogene-free processes (sintering) followed by incubations in aqueous media at temperatures high enough to prevent microbial proliferation (e.g. 80 °C). Thus, it is believed that the presented method could be used industrially to produce DCP scaffolds.

Last but not least, it has to be mentioned that several authors have used a similar approach as the one presented here. For example, Kitamura et al. [45] converted α -TCP scaffolds to octocalcium phosphate in a pH 4.0 buffer solution at 36.5 °C. These authors also observed the formation of nanosized crystals, a decrease of macroporosity, and an increase of specific surface area (from 0.1 to 50 m²/g). However, since the focus of their study was the enhancement of protein adsorption, a detailed description of the reaction kinetics,

change of porosity and mechanical properties was not provided. The group of Ishikawa et al. [46,47] transformed α -TCP granules and blocks hydro thermally in water or disodium carbonate solution to form apatite and carbonated apatite scaffolds, respectively.

5. Conclusion

The goal of the present study was to assess the possibility to convert β -TCP scaffolds into DCP without macrostructural changes. For that purpose, β -TCP scaffolds were first converted to α -TCP via a thermal treatment, and then dipped into a phosphoric acid solution. The results demonstrated that the scaffolds were fully converted to DCP within 2–3 days. The two successive conversion reactions provoked a decrease of porosity from roughly 75 down to 65%. However, only few geometrical changes were seen at the macro-level, i.e. some macropores were partially filled with DCP, hence reducing the mean pore size. Most geometrical changes were observed at the micro-level with the filling of micropores with small DCP crystals. To conclude, the presented method can be used to convert β -TCP scaffolds into DCP scaffolds practically without macrostructural changes and with a positive effect on the mechanical properties (two-fold increase) and the specific surface area (roughly 20-fold increase up to $5 \text{ m}^2/\text{g}$).

Acknowledgments

The authors would like to thank Sonja Grünenfelder and Alfred Benoit for the synthesis of β -TCP porous scaffolds, Werner Hirsiger for the SEM photos, Nicola Doebelin for the help in analyzing the XRD results, and Fabrizio Bigolin for the compressive strength measurements.

References

- [1] Banwart JC, Asher MA, Hassanein RS. Iliac crest bone graft harvest donor site morbidity. A statistical evaluation. *Spine* 1995;20(9):1055–60.
- [2] Younger EM, Chapman MW. Morbidity at bone graft donor sites. *J Orthop Trauma* 1989;3(3):192–5.
- [3] Driskell T. Calcium phosphate resorbable ceramics: a potential alternative to bone grafting. *J Dent Res* 1973;123.
- [4] LeGeros RZ. Calcium phosphate materials in restorative dentistry: a review. *Adv Dent Res* 1988;2(1):164–80.
- [5] Brown WE, Chow LC. A new calcium phosphate setting cement. *J Dent Res* 1983;62:672.
- [6] Bohner M, Gbureck U, Barralet JE. Technological issues for the development of more efficient calcium phosphate bone cements: a critical assessment. *Biomaterials* 2005;26(33):6423–9.
- [7] Mainard D, Gouin F, Chauveaux D, Loty B, editors. *Les substituts osseux en 2003*. Romillat; 2003.
- [8] Frankenburg EP, Goldstein SA, Bauer TW, Harris SA, Poser RD. Biomechanical and histological evaluation of a calcium phosphate cement. *J Bone Joint Surg Am* 1998;80(8):1112–24.
- [9] Gauthier O, Boulter JM, Weiss P, Bosco J, Daculsi G, Aguado E. Kinetic study of bone ingrowth and ceramic resorption associated with the implantation of different injectable calcium-phosphate bone substitutes. *J Biomed Mater Res* 1999;47(1):28–35.
- [10] Barralet JE, Grover L, Gaunt T, Wright AJ, Gibson IR. Preparation of macroporous calcium phosphate cement tissue engineering scaffold. *Biomaterials* 2002;23(15):3063–72.
- [11] Bohner M. Calcium phosphate emulsions: possible applications. *Key Eng Mater* 2001;192–195:765–8.
- [12] Fukase Y, Eanes ED, Takagi S, Chow LC, Brown WE. Setting reactions and compressive strengths of calcium phosphate cements. *J Dent Res* 1990 Dec; 69(12):1852–6.
- [13] LeGeros RZ. Properties of osteoconductive biomaterials: calcium phosphates. *Clin Orthop* 2002;395:81–98.
- [14] Bohner M. Calcium orthophosphates in medicine: from ceramics to calcium phosphate cements. *Injury* 2000;31(Suppl. 4):37–47.
- [15] Kamakura S, Sasano Y, Homma H, Suzuki O, Kagayama M, Motegi K. Implantation of octacalcium phosphate (OCP) in rat skull defects enhances bone repair. *J Dent Res* 1999;78(11):1682–7.
- [16] Ohura K, Bohner M, Hardouin P, Lemaître J, Pasquier G, Flautre B. Resorption of, and bone formation from, new beta-tricalcium phosphate–monocalcium phosphate cements: an in vivo study. *J Biomed Mater Res* 1996;30(2):193–200.
- [17] Suzuki O, Nakamura M, Miyasaka Y, Kagayama M, Sakurai M. Bone-formation on synthetic precursors of hydroxyapatite. *Tohoku J Exp Med* 1991;164(1):37–50.
- [18] Takagi S, Chow LC. Formation of macropores in calcium phosphate cement implants. *J Mater Sci Mater Med* 2001;12(2):135–9.
- [19] del Valle S, Miño N, Muñoz F, González A, Planell JA, Ginebra MP. In vivo evaluation of an injectable macroporous calcium phosphate cement. *J Mater Sci Mater Med* 2007;18(2):353–61.
- [20] Habibovic P, Gbureck U, Doillon CJ, Bassett DC, van Blitterswijk CA, Barralet JE. Osteoconduction and osteoinduction of low-temperature 3D printed bio-ceramic implants. *Biomaterials* 2008;29(7):944–53.
- [21] Ohura K, Hamanishi C, Tanaka S, Matsuda N. Healing of segmental bone defects in rats induced by a beta-TCP–MCPM cement combined with rhBMP-2. *J Biomed Mater Res* 1999;44(2):168–75.
- [22] Tamimi F, Torres J, Kathan C, Baca R, Clemente C, Blanco L, et al. Bone regeneration in rabbit calvaria with novel monetite granules. *J Biomed Mater Res A* 2008. doi:10.1002/jbm.a.31842.
- [23] Enderle R, Gotz-Neunhoeffer F, Gobbels M, Muller FA, Greil P. Influence of magnesium doping on the phase transformation temperature of beta-TCP ceramics examined by Rietveld refinement. *Biomaterials* 2005;26(17):3379–84.
- [24] Bohner M, van Lenthe GH, Grunfelder S, Hirsiger W, Evison R, Muller R. Synthesis and characterization of porous beta-tricalcium phosphate blocks. *Biomaterials* 2005;26:6099–105.
- [25] Hildebrand T, Laib A, Muller R, Dequeker J, Rueggsegger P. Direct three-dimensional morphometric analysis of human cancellous bone: microstructural data from spine, femur, iliac crest, and calcaneus. *J Bone Miner Res* 1999;14(7): 1167–74.
- [26] van Lenthe GH, Hagemuller H, Bohner M, Hollister SJ, Meinel L, Muller R. Nondestructive micro-computed tomography for biological imaging and quantification of scaffold–bone interaction in vivo. *Biomaterials* 2007;28(15): 2479–90.
- [27] Rodriguez-Carvajal J, editor. *FullProf.2k*. 3.40; 2004.
- [28] Schroeder LW, Dickens B, Brown WE. Crystallographic studies of the role of Mg as a stabilizing impurity in β - $\text{Ca}_3(\text{PO}_4)_2$. II. Refinement of Mg-containing β - $\text{Ca}_3(\text{PO}_4)_2$. *J Solid State Chem* 1977;22(3):253–62.
- [29] Mathew M, Schroeder LW, Dickens B, Brown WE. The crystal structure of α - $\text{Ca}_3(\text{PO}_4)_2$. *Acta Crystallogr* 1977;B33:1325–33.
- [30] Dickens B, Bowen JS, Brown WE. A refinement of the crystal structure of CaHPO_4 (synthetic monetite). *Acta Crystallogr* 1971;B28:797–806.
- [31] Curry NA, Jones DW. Crystal structure of brushite, calcium hydrogen orthophosphate dihydrate: a neutron-diffraction investigation. *J Chem Soc A Inorg Phys Theor* 1971:3725–9.
- [32] Klawitter JJ, Hulbert SF. Application of porous ceramics for the attachment of load bearing internal orthopedic applications. *J Biomed Mater Res Symp* 1971; 2(1):161–229.
- [33] Lu JX, Flautre B, Anselme K, Hardouin P, Gallur A, Descamps M, et al. Role of interconnections in porous bioceramics on bone recolonization in vitro and in vivo. *J Mater Sci Mater Med* 1999;10(2):111–20.
- [34] Mastrogiacomo M, Scaglione S, Martinetti R, Dolcini L, Beltrame F, Cancedda R, et al. Role of scaffold internal structure on in vivo bone formation in macroporous calcium phosphate bioceramics. *Biomaterials* 2006;27(17):3230–7.
- [35] von Doernberg MC, von Rechenberg B, Bohner M, Grunfelder S, van Lenthe GH, Muller R, et al. In vivo behavior of calcium phosphate scaffolds with four different pore sizes. *Biomaterials* 2006;27(30):5186–98.
- [36] Vereecke G, Lemaître J. Calculation of the solubility diagrams in the system $\text{Ca}(\text{OH})_2$ – H_3PO_4 – KOH – HNO_3 – CO_2 – H_2O . *J Cryst Growth* 1990;104:820–32.
- [37] Frêche M, Heughebaert JC. Calcium phosphate precipitation in the 60–80 °C range. *J Cryst Growth* 1989;94:947–54.
- [38] Kosar-Grasic B, Purgaric B, Füredi-Milhofer H. Precipitation of calcium phosphates from electrolyte solutions – VI. The precipitation diagram of calcium hydrogen phosphate. *J Inorg Nucl Chem* 1978;40:1877–80.
- [39] Martin RB, Brown PW. Phase equilibria among acid calcium phosphates. *J Am Ceram Soc* 1997;80:1263–6.
- [40] Bohner M, Merkle HP, Lemaître J. In vitro aging of a calcium phosphate cement. *J Mater Sci Mater Med* 2000;11:155–62.
- [41] Dugleux P, de Sallier Dupin A. Contribution à l'étude cinétique de la déshydratation du phosphate bicalcique. II. – Déshydratation de $\text{CaHPO}_4 \cdot 2\text{H}_2\text{O}$ en ambiance sèche ou légèrement humide. *Bull Soc Chim Fr* 1967;3:973–8.
- [42] Dugleux P, de Sallier Dupin A. Contribution à l'étude cinétique de la déshydratation du phosphate bicalcique. III. – Interprétation des résultats, ébauche du mécanisme réactionnel. *Bull Soc Chim Fr* 1967;3:978–82.
- [43] Dugleux P, de Sallier Dupin A. Contribution à l'étude cinétique de la déshydratation du phosphate bicalcique. I. – Déshydratation de $\text{CaHPO}_4 \cdot 2\text{H}_2\text{O}$ en atmosphère de vapeur d'eau. *Bull Soc Chim Fr* 1967;1:144–50.
- [44] Charrière E, Terrazzoni S, Pittet C, Mordasini PH, Dutoit M, Lemaître J, et al. Mechanical characterization of brushite and hydroxyapatite cements. *Biomaterials* 2001;22(21):2937–45.
- [45] Kitamura M, Ohtsuki C, Ogata S-I, Kamitakahara M, Tanihara M, Miyazaki T. Mesoporous calcium phosphate via post-treatment of α -TCP. *J Am Ceram Soc* 2005;88(4):822–6.
- [46] Ishikawa K, Karashima S, Takeuchi A, Matsuya S. Apatite foam fabrication based on hydrothermal reaction of α -tricalcium phosphate foam. *Key Eng Mater* 2008;361–363:319–22.
- [47] Wakae H, Takeuchi A, Matsuya S, Munar ML, Nakagawa M, Udoh K-I, et al. Effects of hydrothermal treatment temperature on the crystallinity of cancellous bone type carbonate apatite foam. *Key Eng Mater* 2008;361–363: 975–8.